An enrichment scheme for solidification problems

Alejandro Cosimo, Víctor Fachinotti & Alberto Cardona

Computational Mechanics
Solids, Fluids, Structures, Fluid-Structure Interactions, Biomechanics, Micromechanics, Multiscale Mechanics, Materials, Constitutive Modeling, Nonlinear Mechanics, Aerodynamics

ISSN 0178-7675

Comput Mech
DOI 10.1007/s00466-012-0792-9

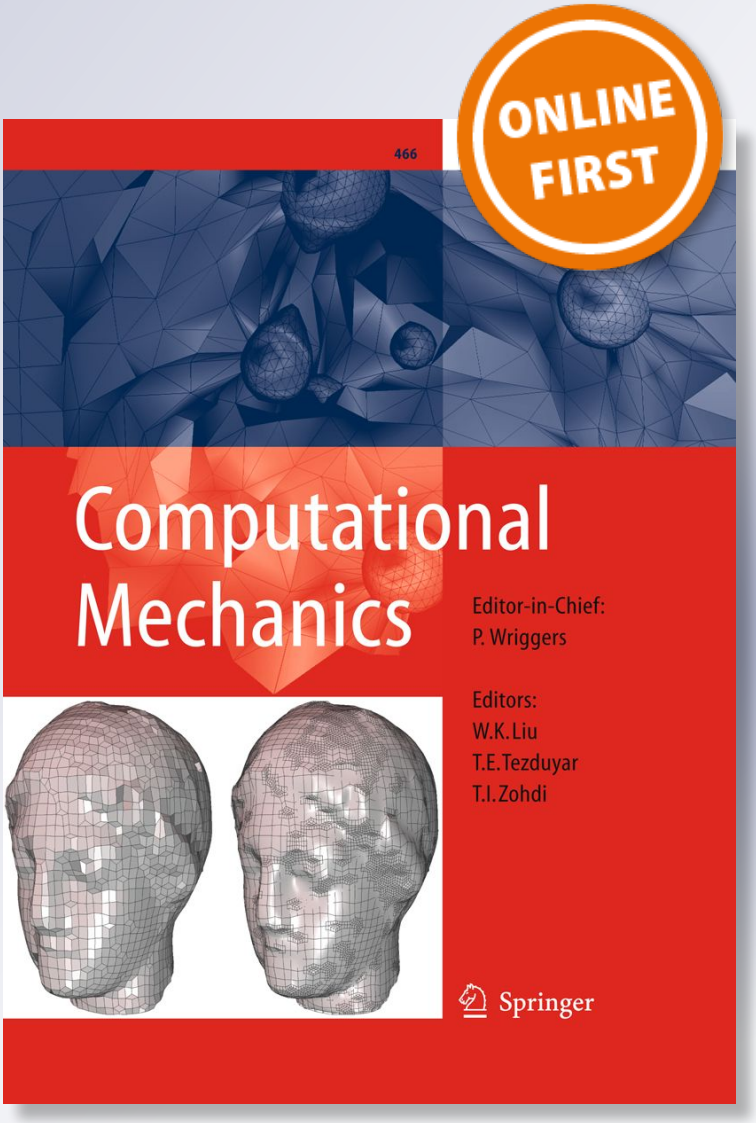

Springer

Your article is protected by copyright and all rights are held exclusively by Springer-Verlag. This e-offprint is for personal use only and shall not be self-archived in electronic repositories. If you wish to self-archive your work, please use the accepted author's version for posting to your own website or your institution's repository. You may further deposit the accepted author's version on a funder's repository at a funder's request, provided it is not made publicly available until 12 months after publication.

Springer

Author's personal copy

Comput Mech
DOI 10.1007/s00466-012-0792-9

ORIGINAL PAPER

An enrichment scheme for solidification problems

Alejandro Cosimo · Víctor Fachinotti · Alberto Cardona

Received: 16 April 2012 / Accepted: 3 September 2012
© Springer-Verlag 2012

Abstract A new enriched finite element formulation for solving isothermal phase change problems is presented. We propose a fixed mesh method, where the discontinuity in the temperature gradient is represented by enriching the finite element space through a function whose definition includes a gradient discontinuity. Generally, in these types of formulations, the enrichment location (the location of the solidification front) is determined through a level set auxiliary scheme. In this work, this position is determined implicitly by constraining the temperature at the phase change boundary to be equal to the melting temperature. Several numerical examples are presented to show the application of the method.

Keywords Enriched finite element method · Solidification problems · Stefan problem · Phase change problems · XFEM

1 Introduction

Solidification processes are of interest in many areas of engineering, such as welding mechanics, nuclear engineering, metallurgy and metal casting processes [2,5,13,23,25]. When considering solidification of a pure substance, problems are described as isothermal phase change problems that are characterised mainly by two parameters: the material melting temperature and its latent heat. An inherent difficulty with these problems is the discontinuity in the temperature gradient at the solidification front.

From a general point of view, two specialisations of the finite element method (FEM) are aimed at solving phase change problems: moving mesh or front tracking methods and fixed mesh methods [19]. Moving mesh methods track the position of the phase change boundary; therefore, through remeshing, the mesh conforms to the position of the interface. In this way, the FEM formulation addresses the weak discontinuity present in the temperature field at the solidification front in a standard way, which is presented in several studies [4,6,26]. The problem with this type of methods is that in multidimensional problems, the mesh can become too distorted as the interface evolves. This does not occur with fixed mesh methods. Different types of fixed mesh methods were proposed, i.e., enthalpy methods [36,38], capacitance methods [30] and temperature based methods [8,11,14,35]. However, none of these methods is able to represent the gradient discontinuity at the phase change boundary.

Because of the mesh distortion problem and the need for remeshing of the front tracking methods, we propose a fixed mesh scheme, which represents the aforementioned discontinuity. This method has the advantages of both groups of methods: the ability to represent the weak discontinuity without mesh distortions.

In classical fixed mesh methods, loss of stability and/or robustness, which are associated with discontinuity at the interface, appears with low sensible to latent heat ratios (Stefan number) or when the initial temperature is close to the melting temperature [31]. These situations cannot be handled efficiently and require a large number of elements for accurate solutions. In several scenarios, the standard Newton–Raphson solver does not converge and a line search must be used [28].

A. Cosimo (✉) · V. Fachinotti · A. Cardona
Centro Internacional de Métodos Computacionales en Ingeniería (CIMEC-INTEC), Universidad Nacional del Litoral-CONICET, Güemes 3450, S3000GLN Santa Fe, Argentina
e-mail: alecosimo@gmail.com

V. Fachinotti
e-mail: vfachino@intec.unl.edu.ar

A. Cardona
e-mail: acardona@intec.unl.edu.ar

Published online: 18 September 2012

Author's personal copy

Fixed mesh finite element formulations that perform discontinuous spatial integration, such as those proposed by Crivelli and Idelsohn [11] and subsequently refined by Storti et al. [35] and Fachinotti et al. [14], provide spurious oscillations in the computed solution for certain situations. This phenomenon appears for high latent heat values because the discontinuity in the temperature gradient at the interface is pronounced and cannot be represented when the position of the solidification front does not coincide with an element boundary due to the continuous interpolated gradient inside the element. This situation is worse with linear shape functions, which are used in most cases with discontinuous integration, resulting in a space of trial solutions that can reproduce up to piecewise constant gradients. One approach to avoid this situation is to introduce the representation of the gradient discontinuity by enriching the element. Another approach, proposed recently by Davey and Mondragon [12], involves removing the discontinuity through the introduction of a non-physical enthalpy.

Currently, enriching techniques are widely used in fluid and fracture mechanics [3,16,33]. These techniques are designed to represent the existing discontinuities and singularities in the fields of interest. If we apply the usual techniques in these situations (e.g., standard finite element formulations), the overall convergence rate is not optimal in the sense described by Fries [15].

Although new enriched formulations are constantly being proposed, it should be noted that this is not the case for solidification problems. There are few enriched formulations in the literature for solving the previously mentioned types of phase change problems. Chessa et al. [9] and Bernauer and Herzog [7] determined the position of the enrichment through a level set function that is evolved with the interface Rankine–Hugoniot condition (specialised to the Stefan problem) and the associated advection equation. Several steps are performed to compute the solution of the level set equation [32]. First, the velocity of the solidification front is computed from the Stefan condition, and a velocity field is built by extending the velocity of the solidification front to the whole domain. Next, the level set equation is solved to move the interface. Finally, the standard heat equation is solved for each domain (solid and liquid) separately by imposing the interface constraint that dictates that the temperature at the phase change boundary must be equal to the melting temperature. The imposition of the mentioned constraint is enforced with a penalty formulation or a Lagrange multipliers formulation. Ji et al. [20] present a similar approach, differing from the previous one in the level set update and the energetically consistent way that they use to determine the jump in the heat flux at the interface. In contrast, Merle and Dolbow [27] proposed an enriched formulation in which they use an equation that is similar to a level set to track the interface position and the LATIN method [24] as iterative procedure to satisfy the local interface constraints stated by the problem.

In this study, the Stefan condition is satisfied with the weak formulation of the problem. This is accomplished with a weak formulation of the problem in each subdomain (liquid and solid). The Reynold's theorem is applied to extend the formulation to the whole domain and to satisfy the Stefan condition as an internal natural phase change boundary condition. Next, the interface position is determined implicitly during the simulation with the aforementioned constraint in the temperature at the solidification front. The formulation is performed while considering the enriched space. In this way, the overhead introduced by the classical level set methods is avoided and no auxiliary equation (e.g., the level set equation) is required.

The discrete formulation is completely stated for the one dimensional case and a discussion for the extension to two dimensions is given. The one dimensional implementation is tested for extreme values of temperature gradient discontinuity and for initial temperatures close to the melting temperature. The results obtained for one of the examples are contrasted against those obtained by other enriched formulations [27]. Also, comparisons with results obtained using a non enriched fixed mesh numerical scheme [14], where the temperature gradient discontinuity is not considered, are presented. Finally, conclusions are presented.

2 Mathematical setting

Isothermal phase change problems are governed by the first principle of thermodynamics. Assuming the contribution of the mechanical energy to the total energy negligible and considering the specific enthalpy $\mathcal{H}$ as a thermodynamic potential, the temperature field T is computed by solving the heat balance equation

$$\rho\dot{\mathcal{H}} = Q + \nabla\cdot(k\nabla T) \qquad \forall(\boldsymbol{x},t)\in\Omega_i\times(t_0,\infty) \tag{1}$$

where ρ is the density, k is the thermal conductivity, T is the temperature, Q is the external heat source per unit volume, and Ω_i for $i\in[s,l]$ are the solid and liquid sub-domains with $\Omega_s\cap\Omega_l=\{\emptyset\}$ and $\Omega=\Omega_s\cup\Omega_l$. The temperature field should verify the initial conditions

$$T = T_0 \qquad \forall\boldsymbol{x}\in\Omega, t=t_0 \tag{2}$$

where $T_0(\boldsymbol{x})$ is the given initial temperature field. Additionally, the following set of conditions must be verified at the disjoint portions Γ_d, Γ_q, Γ_c of the external boundary:

$$T = T_d \quad \forall\,(\boldsymbol{x},t)\in\Gamma_d\times(t_0,\infty) \tag{3}$$

$$-(k\nabla T)\cdot\boldsymbol{n} = q_w \quad \forall\,(\boldsymbol{x},t)\in\Gamma_q\times(t_0,\infty) \tag{4}$$

$$-(k\nabla T)\cdot\boldsymbol{n} = h_f(T-T_f)\ \forall(\boldsymbol{x},t)\in\Gamma_c\times(t_0,\infty) \tag{5}$$

Author's personal copy

where $\Gamma_d \cup \Gamma_q \cup \Gamma_c = \partial\Omega$, and where T_d is the imposed temperature at the boundary Γ_d, q_w is the external heat flow at the boundary Γ_q, h_f is the heat convection coefficient, T_f is the external fluid temperature at the portion the boundary Γ_c and $\boldsymbol{n}$ is the outward normal to the boundary under consideration. Finally, at the interface Γ between Ω_s and Ω_l (the phase change boundary), the constraint on the temperature and the Stefan condition hold

$$T = T_m \qquad \forall(\boldsymbol{x}, t) \in \Gamma \times (t_0, \infty) \tag{6}$$

$$[-(k\nabla T)\cdot \boldsymbol{n}_\Gamma]_\Gamma = \rho\mathcal{L}u_\Gamma \qquad \forall(\boldsymbol{x}, t) \in \Gamma \times (t_0, \infty). \tag{7}$$

Here, $\mathcal{L}$ is the latent heat, T_m is the melting temperature, $\boldsymbol{n}_\Gamma$ is the outward normal to the solidification front from the solid domain, $u_\Gamma = \boldsymbol{u}_\Gamma \cdot \boldsymbol{n}_\Gamma$ is the velocity of the interface in the direction of the normal $\boldsymbol{n}_\Gamma$ and the operator $[\boldsymbol{.}]_\Gamma$ measures the jump of the quantity $\boldsymbol{.}$ at the solidification front. Equation (6) is the constraint that imposes that the temperature at the phase change boundary must be equal to the melting temperature and Eq. (7) is the interface condition (the Stefan condition).

2.1 Variational temperature based formulation

Let $\mathcal{S} = \{T/T \in \mathcal{H}^1(\Omega),\ T|_{\Gamma_d} = T_d\}$ be the space of trial solutions and $\mathcal{V} = \{v/v \in \mathcal{H}^1(\Omega),\ v|_{\Gamma_d} = 0\}$ be the space of weighting or test functions, where $\mathcal{H}^1$ is the first order Sobolev space. By integrating Eq. (1) separately in each subdomain (solid and liquid), the following weak form is obtained

$$\sum_{i\in[s,l]} \int_{\Omega_i} w\left[\rho\dot{\mathcal{H}} - \nabla\cdot(k\nabla T) - Q\right] d\Omega = 0 \tag{8}$$

with $w \in \mathcal{V}$ and $T \in \mathcal{S}$. After applying the divergence theorem and replacing the boundary conditions from Eqs. (3–5), we obtain

$$\begin{aligned}\sum_i \int_{\Omega_i} w\left[\rho\dot{\mathcal{H}} - Q\right] d\Omega + \sum_i \int_{\Omega_i} \nabla w\cdot(k\nabla T)\, d\Omega \\ - \sum_i \int_{\Gamma_i} wk\nabla T\cdot \boldsymbol{n}_i\, d\Gamma + \int_{\Gamma_c} wh_f(T - T_f)\, d\Gamma \\ + \int_{\Gamma_q} wq_w\, d\Gamma = 0.\end{aligned} \tag{9}$$

Functions $w \in \mathcal{V}$ depend on time because the enrichment continuously adapts to the position of the interface. By applying the Reynolds theorem to the first term of Eq. (9), we obtain

$$\begin{aligned}\sum_i \int_{\Omega_i} w\rho\dot{\mathcal{H}}\, d\Omega = \sum_i \left[\frac{\partial}{\partial t}\int_{\Omega_i} w\rho\mathcal{H}\, d\Omega \right. \\ \left. - \int_{\Omega_i} \rho\mathcal{H}\dot{w}\, d\Omega - \int_{\Gamma_i} w\rho\mathcal{H}\boldsymbol{u}_i\cdot\boldsymbol{n}_i\, d\Gamma\right]\end{aligned} \tag{10}$$

where $\boldsymbol{u}_i$ is the velocity of the boundary Γ_i and $\boldsymbol{n}_i$ is the external unit normal vector of that boundary. Taking into account that the latent heat represents the jump of the enthalpy at the phase change boundary Γ, we have $\mathcal{L} = [\mathcal{H}]_\Gamma$. Then, the last term of the last equation becomes

$$\begin{aligned}\sum_i \int_{\Gamma_i} w\rho\mathcal{H}\boldsymbol{u}_i\cdot\boldsymbol{n}_i\, d\Gamma &= \int_\Gamma w\rho\mathcal{L}u_\Gamma\, d\Gamma \\ &= -\sum_i \int_{\Gamma_i} wk\nabla T\cdot\boldsymbol{n}_i\, d\Gamma.\end{aligned} \tag{11}$$

Replacing Eq. (11) into (10) and using this result in Eq. (9), we obtain

$$\begin{aligned}\sum_i \left[\frac{\partial}{\partial t}\int_{\Omega_i} w\rho\mathcal{H}\, d\Omega - \int_{\Omega_i} \rho\mathcal{H}\dot{w}\, d\Omega \right. \\ \left. - \int_{\Omega_i} wQ\, d\Omega + \int_{\Omega_i} \nabla w\cdot(k\nabla T)\, d\Omega\right] \\ + \int_{\Gamma_c} wh_f(T - T_f)\, d\Gamma + \int_{\Gamma_q} wq_w\, d\Gamma = 0.\end{aligned} \tag{12}$$

The Stefan condition is therefore satisfied in weak form.

Then, the addition of the first two terms of the last equation gives

$$\begin{aligned}\sum_i \left[\frac{\partial}{\partial t}\int_{\Omega_i} w\rho\mathcal{H}\, d\Omega - \int_{\Omega_i} \rho\mathcal{H}\dot{w}\, d\Omega\right] \\ = \frac{\partial}{\partial t}\int_\Omega w\rho\mathcal{H}\, d\Omega - \int_\Omega \rho\mathcal{H}\dot{w}\, d\Omega = \int_\Omega w\rho\dot{\mathcal{H}}\, d\Omega.\end{aligned} \tag{13}$$

Using this result into Eq. (12), we obtain

$$\begin{aligned}\int_\Omega w\left[\rho\dot{\mathcal{H}} - Q\right] d\Omega + \int_\Omega \nabla w\cdot(k\nabla T)\, d\Omega \\ + \int_{\Gamma_c} wh_f(T - T_f)\, d\Gamma + \int_{\Gamma_q} wq_w\, d\Gamma = 0.\end{aligned} \tag{14}$$

The specific enthalpy $\mathcal{H}$ can be expressed in terms of the temperature T as

$$\mathcal{H}(T) = \int_{T_{\text{ref}}}^{T} c(\tau)d\tau + \mathcal{L}f_l(T) \tag{15}$$

Author's personal copy

where T_{ref} is a reference temperature, $c(\tau) \equiv c$ is the heat capacity and $f_l(T)$ is the liquid fraction. For isothermal phase change, the liquid fraction is expressed as a Heaviside step, i.e. $f_l = H_{eav}(T - T_m)$.

Finally, by replacing Eq. (15) into (14), the following temperature based variational formulation is obtained

Find $T \in \mathcal{S}$ such that $\forall w \in \mathcal{V}$

$$\int_\Omega w\left[\rho c\frac{\partial T}{\partial t}+\rho\mathcal{L}\frac{\partial f_l}{\partial t}-Q\right]\,d\Omega+\int_\Omega \nabla w\cdot(k\nabla T)\,d\Omega$$
$$+\int_{\Gamma_c} wh_f(T-T_f)\,d\Gamma+\int_{\Gamma_q} wq_w\,d\Gamma=0,\ \text{for } t>0;$$
$$\int_\Omega wT\,d\Omega=\int_\Omega wT_0\,d\Omega\,,\qquad \text{for } t=0. \tag{16}$$

We remark that, in the case of isothermal phase change, the time derivative of the liquid fraction $\frac{\partial f_l}{\partial t}$ should be interpreted in a distributional sense.

3 Enriched finite element formulation

For solidification problems, there is a weak discontinuity, i.e. only the gradient of the temperature field is discontinuous at the solidification front. The main features of this discontinuity are its weakness and local behaviour. For the local behaviour, we only need to enrich those elements that are crossed by the phase change boundary. For the weak discontinuity, the enrichment function only needs to have a discontinuity in its gradient.

A Galerkin finite element formulation is adopted for the discretisation of the continuous variational formulation. The enrichment functions are time dependent because of the change in position of the interface. Therefore, the space of weighting functions $\mathcal{V}$ depends on time, and the spatial and time discretisations need to be studied carefully. Following Fries and Zillian [17], the discretisation in time is first performed, and then the space discretisation is performed.

The functional space of the element intersected by the interface (or solidification front) is enriched with a weak discontinuous function denoted by E. From the previous comments, two features need to be considered to build this function: E should have a local character and should vanish at the element nodes, and ∇E must be discontinuous at the phase change boundary. An enrichment function with these features was proposed by Coppola-Owen and Codina [10].

3.1 Time discretisation

An unconditionally stable backward Euler scheme is used to accomplish the temporal discretisation, obtaining the following result

$$\int_\Omega w_n\left[\rho c_n\frac{T_n-T_{n-1}}{\Delta t}+\rho\mathcal{L}\frac{f_{l(n)}-f_{l(n-1)}}{\Delta t}\right]d\Omega$$
$$-\int_\Omega\left[\nabla w_n\cdot(k_n\nabla T_n)+wQ_n\right]d\Omega+\int_{\Gamma_q} w_nq_{w_n}\,d\Gamma$$
$$+\int_{\Gamma_c} w_nh_{f_n}(T_n-T_{f_n})\,d\Gamma=0 \tag{17}$$

where $c_n \equiv c(T_n)$, $k_n \equiv k(T_n)$, $h_{f_n} \equiv h_f(T_n)$ and $q_{w_n} \equiv q_w(T_n)$.

The time level for the evaluation of the test function w was specified in a consistent way at time t_n, i.e. $w(\boldsymbol{x}, t_n) \equiv w_n$. We remark that if w was evaluated at the time level $n-1$, the regularity of the system matrix could not be guaranteed [17].

To elucidate this issue, consider the case where at time step $n-1$ the phase change boundary is within element e, and at time step n the phase change boundary is within the neighboring element $e+1$. At time t_{n-1}, element e is enriched whereas element $e+1$ is not. When the interface tries to evolve to element $e+1$, the weight function w_{n-1} is zero at that element, providing a null equation for the enrichment. Therefore, the system matrix would be singular.

3.2 Spatial discretisation

Let $\mathcal{S}^h \subset \mathcal{S}$ and $\mathcal{V}^h \subset \mathcal{V}$ be N-dimensional subspaces of the trial and test functional spaces, formed by the usual finite element space *and* the enrichment functions. The discrete variational formulation is given by

Given T^h_{n-1}, find $T^h_n = v^h + T^h_d$, where $v^h \in \mathcal{V}^h$ and $T^h_n|_{\Gamma_d} = T^h_d$, such that $\forall w^h_n \in \mathcal{V}^h$

$$\int_\Omega w^h_n\left[\rho c_n\frac{T^h_n-T^h_{n-1}}{\Delta t}+\rho\mathcal{L}\frac{f_{l(n)}-f_{l(n-1)}}{\Delta t}\right]d\Omega$$
$$-\int_\Omega\left[\nabla w^h_n\cdot(k_n\nabla T^h_n)+w^h_nQ_n\right]d\Omega$$
$$+\int_{\Gamma_q} w^h_nq_{w_n}\,d\Gamma+\int_{\Gamma_c} w^h_nh_{f_n}(T^h_n-T_{f_n})\,d\Gamma=0\,,$$
$$\text{for } n=1,2,3,\ldots$$
$$\int_\Omega w^h_0T^h_0\,d\Omega=\int_\Omega w^h_0T_0\,d\Omega\qquad\text{for } n=0. \tag{18}$$

For conciseness, it is assumed without loss of generality that $T^h_d = 0$, such that $T^h_n = v^h$. Then Eq. (18) can be written as

Author's personal copy

$$\frac{1}{\Delta t}\int_{\Omega}\rho c_n w_n^h T_n^h\, d\Omega - \frac{1}{\Delta t}\int_{\Omega}\rho c_n w_n^h T_{n-1}^h\, d\Omega + \frac{1}{\Delta t}\int_{\Omega}\rho\mathcal{L} w_n^h f_{l(n)}^h\, d\Omega - \frac{1}{\Delta t}\int_{\Omega}\rho\mathcal{L} w_n^h f_{l(n-1)}^h\, d\Omega + \int_{\Omega} k_n \nabla T_n^h \cdot \nabla w_n^h\, d\Omega - \int_{\Omega} Q_n^h w_n^h\, d\Omega + \int_{\Gamma_q} w_n^h q_w\, d\Gamma + \int_{\Gamma_c} w_n^h h_{f_n} T_n^h\, d\Gamma + \int_{\Gamma_c} w_n^h h_{f_n} T_{f(n)}\, d\Gamma = 0. \tag{19}$$

The discrete test and trial functions $v^h \in \mathcal{V}^h$ are the set of usual linear finite element functions covering the whole domain, plus the enrichment functions at the elements that are crossed by the interface. Thus, a typical enriched finite element in the one dimensional case has a total of three shape functions (including the enrichment one). In matrix notation, $T^h \in \mathcal{V}^h$ inside an enriched element is given by

$$T^h = \boldsymbol{N}^T \boldsymbol{T}, \tag{20}$$

where $\boldsymbol{N}$ denotes the shape functions and $\boldsymbol{T}$ the degrees of freedom amplitudes.

The contribution of an enriched element to the residual at time t_n, is obtained next from Eq. (19):

$$\boldsymbol{\Pi} = \frac{\boldsymbol{C}\boldsymbol{T}_n}{\Delta t} - \frac{\boldsymbol{C}^*\boldsymbol{T}_{n-1}}{\Delta t} + \frac{\boldsymbol{L}_n - \boldsymbol{L}_{n-1}}{\Delta t} + \boldsymbol{K}\boldsymbol{T}_n + \boldsymbol{F} - \boldsymbol{Q} \tag{21}$$

where

$$\boldsymbol{C} = \int_{\Omega}\rho c_n \boldsymbol{N}_n \boldsymbol{N}_n^T\, d\Omega \tag{22}$$

$$\boldsymbol{C}^* = \int_{\Omega}\rho c_n \boldsymbol{N}_n \boldsymbol{N}_{n-1}^T\, d\Omega \tag{23}$$

$$\boldsymbol{K} = \int_{\Omega}\nabla \boldsymbol{N}_n k_n \nabla \boldsymbol{N}_n^T\, \Omega + \int_{\Gamma_c} h_{f_n} \boldsymbol{N}_n \boldsymbol{N}_n^T\, d\Gamma \tag{24}$$

$$\boldsymbol{L}_n = \int_{\Omega}\rho\mathcal{L}\boldsymbol{N}_n f_{l(n)}\, d\Omega \tag{25}$$

$$\boldsymbol{L}_{n-1} = \int_{\Omega}\rho\mathcal{L}\boldsymbol{N}_n f_{l(n-1)}\, d\Omega \tag{26}$$

$$\boldsymbol{F} = \int_{\Gamma_q} \boldsymbol{N}_n q_{w_n}\, d\Gamma - \int_{\Gamma_c} h_{f_n} \boldsymbol{N}_n T_{f_n}\, d\Gamma \tag{27}$$

$$\boldsymbol{Q} = \int_{\Omega} \boldsymbol{N}_n Q_n\, d\Omega. \tag{28}$$

It is worthwhile to mention that function $\boldsymbol{N}_n$ depends on the interface position, which is an unknown of the problem, incrementing the degree of non linearity of the equations. The nonlinear problem (21) is solved using a Newton–Raphson scheme

$$\boldsymbol{\Pi}^{(i+1)} \simeq \boldsymbol{\Pi}^{(i)} + \frac{\partial \boldsymbol{\Pi}}{\partial \boldsymbol{T}}^{(i)} (\boldsymbol{T}^{(i+1)} - \boldsymbol{T}^{(i)}) = \boldsymbol{0} \tag{29}$$

where i represents the ith iteration. Note that we omitted the subscript n to simplify notation.

Iterations proceed until convergence (the norm of the residual meets a prescribed tolerance). Due to the high non linearity of the problem, a line-search method must be used in conjunction with the Newton–Raphson scheme. This type of globally convergent method is quite standard and its formulation can be found in most textbooks that consider nonlinear optimisation problems [21,39].

3.3 Determination of the interface position

The determination of the interface position is essential for this method because the enriched shape functions depend on it.

In other enrichment formulations, the interface position is computed using an auxiliary level set equation. After this position is determined, the standard heat conduction equation is solved in each subdomain, enriching the elements that are intersected by the phase change boundary. Additionally, the constraint (6) is imposed through the use of Lagrange multipliers or a penalty formulation.

We are proposing a new way to determine the interface position implicitly at each Newton iteration, in terms of the values of the degrees of freedom corresponding to that iteration and the constraint given by Eq. (6). Suppose that we are processing iteration i and we have the guess values $\boldsymbol{T}^{(i)}$. With these guess values, we determine if the element that is being processed is intersected by the solidification front. If this is the case, the position of the phase change boundary is computed by using the constraint Eq. (6). A detailed presentation of this issue is given for the one dimensional case in Sect. 3.6.2 and a discussion for the two dimensional case is presented in Sect. 3.7.

3.4 Discontinuous integration

When processing an enriched element, a weak discontinuity appears in the element. In order to evaluate integrals in Eqs. (22–28), a discontinuous integration procedure is used. The number of integration regions depends on the nature of the integrand, i.e. whether the integrand depends only on the time t_n or whether it depends on both time stages t_{n-1} and t_n. In the former case we have two integration subregions,

Author's personal copy

while in the latter case we typically have three integration subregions with a continuous integrand in each of them.

For instance, suppose that we are processing an enriched element, and we are computing the term described by Eq. (23) with three subregions. Then, the elemental contribution $\boldsymbol{C}_e^*$ is given by

$$\boldsymbol{C}_e^* = \int_{\Omega^e} \rho c \boldsymbol{N}_n \boldsymbol{N}_{n-1}^T \, d\Omega = \sum_{p=1}^{3} \int_{\Omega^p} \rho c \boldsymbol{N}_n \boldsymbol{N}_{n-1}^T \, d\Omega \quad (30)$$

where p indicates the partition or region number (ranging in this case from one to three), Ω^p denotes each partition and Ω^e denotes the region of the element. The integration is performed numerically using a Gaussian quadrature in each sub-region [29].

3.5 Tangent matrix

After differentiating the nonlinear residual function (21) with respect to the generalised degrees of freedom $\boldsymbol{T}$, we obtain

$$\frac{\partial \boldsymbol{\Pi}}{\partial \boldsymbol{T}} = \frac{\boldsymbol{C}}{\Delta t} + \boldsymbol{K} + \frac{1}{\Delta t}\frac{\partial \boldsymbol{C}}{\partial \boldsymbol{T}}\boldsymbol{T}^{(i)} - \frac{1}{\Delta t}\frac{\partial \boldsymbol{C}^*}{\partial \boldsymbol{T}}\boldsymbol{T}_{n-1} + \frac{\partial \boldsymbol{K}}{\partial \boldsymbol{T}}\boldsymbol{T}^{(i)} + \frac{1}{\Delta t}\frac{\partial \boldsymbol{L}_n}{\partial \boldsymbol{T}} - \frac{1}{\Delta t}\frac{\partial \boldsymbol{L}_{n-1}}{\partial \boldsymbol{T}} + \frac{\partial \boldsymbol{F}}{\partial \boldsymbol{T}} - \frac{\partial \boldsymbol{Q}}{\partial \boldsymbol{T}}. \quad (31)$$

The first two terms on the right-hand-side are standard in any nonlinear thermal problem. The other terms have certain particularities in the enriched elements, which will be described.

As previously stated, the computation of the mentioned terms in an enriched element depends on the number of subregions. We analyse the case of the term $\frac{\partial \boldsymbol{C}^*}{\partial \boldsymbol{T}}$; the other terms in Eq. (31) are computed similarly.

There are three sources of dependency of $\boldsymbol{C}^*$ on $\boldsymbol{T}$:

- *Evaluation dependency* the integration region depends on the position of the discontinuity at the time stage t_n. Therefore, the position of the Gauss points in the physical space depends implicitly on the degrees of freedom $\boldsymbol{T}$.
- *Enrichment dependency* the position for the enrichment is always determined in terms of the degrees of freedom $\boldsymbol{T}$, so the enrichment function definition depends on $\boldsymbol{T}$.
- *Integration region dependency* when discontinuous integration is applied and the integration region is determined by the position of the interface at time stage t_n. An implicit dependency on the degrees of freedom $\boldsymbol{T}$ is present.

In what follows, a complete description of the computation of the tangent matrix for the one dimensional case is given.

3.6 One dimensional formulation

To evaluate in more detail the proposed ideas, we restrict first the analysis to the one dimensional case. In the numerical examples section we show the application of the one dimensional formulation for a series of problems.

3.6.1 Enrichment function definition

For the definition of the enrichment function we need to know the position of the interface. To describe that position, we make use of a level set function ϕ defined by

$$\phi = x - x_a \quad (32)$$

where x_a is given by

$$x_a = x_1 + s(x_2 - x_1) = x_1 + sh \quad (33)$$

with x_1 the position of the left node, x_2 the position of the right node and h the element length. The interface is located at the point where the level set function ϕ equals zero. This position is provided locally by the parameter $s \in (0, 1)$, while its global position is tracked with x_a.

Then, the definition of the enrichment function is given by

$$E(x) = \begin{cases} \dfrac{x - x_1}{x_a - x_1} = \dfrac{\phi_1 - \phi}{\phi_1} & x \le x_a \\ \dfrac{x_2 - x}{x_2 - x_a} = \dfrac{\phi_2 - \phi}{\phi_2} & x > x_a \end{cases} \quad (34)$$

where $\phi_1 = x_1 - x_a$ and $\phi_2 = x_2 - x_a$. The temperature field inside an enriched element is described as

$$T^h(x, t) = \sum_i N_i(x) T_i + E(x, t) a \quad (35)$$

where the term $\sum N_i T_i$ corresponds to the usual finite element discretisation with N_i the shape functions and T_i the nodal degrees of freedom. The term $E(x, t)a$ corresponds to the enrichment, where $E(x, t)$ is the enrichment function and a is the associated degree of freedom. In the subsequent development linear shape functions are used. In matrix notation, $T^h \in \mathcal{V}^h$ inside an enriched element is given by

$$T^h = \boldsymbol{N}^T \boldsymbol{T} \quad (36)$$

where

$$\boldsymbol{N} = \begin{bmatrix} N_1(x) \\ N_2(x) \\ E(x, t) \end{bmatrix} \quad \text{and} \quad \boldsymbol{T} = \begin{bmatrix} T_1 \\ T_2 \\ a \end{bmatrix}. \quad (37)$$

An example of the previously described enrichment function is provided in Fig. 1, with a discontinuity at $s = 0.35$. For one dimensional cases, this enrichment is conforming but this is not true for higher dimensions.

Author's personal copy

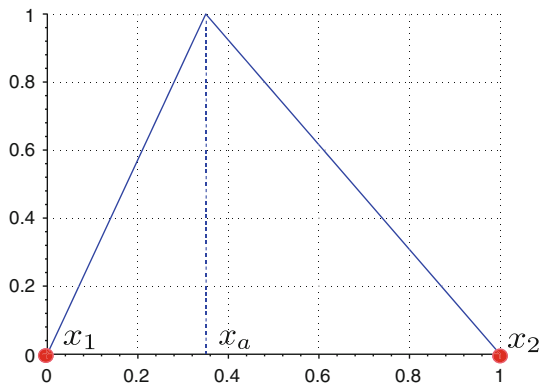

Fig. 1 One dimensional enrichment function

3.6.2 Determination of the interface position

As it was previously introduced to determine the interface position we apply the constraint given by equation (6). When using the enrichment function defined in equation (34), a closed form of the value of the parameter s can be determined, which is given by

$$s = \frac{T_m - T_1^{(i)} - a^{(i)}}{T_2^{(i)} - T_1^{(i)}}. \tag{38}$$

Note that this procedure is based on physical features more than other methods due to determination of the interface position with the current temperature distribution.

3.6.3 Tangent matrix

In this section we consider the case in which thermophysical properties do not depend on temperature. Contributions to the tangent matrix arising from temperature dependent thermophysical properties are considered in Sect. 3.6.4.

Considering the outlined dependencies in Sect. 3.5 and the example of the derivative $\frac{\partial \boldsymbol{C}^*}{\partial \boldsymbol{T}}$, the Gauss numerical discontinuous integration of Eq. (30) for the one dimensional case is given by

$$\begin{aligned} \boldsymbol{C}_e^* &= \int_{\Omega^e} \rho c \boldsymbol{N}_n \boldsymbol{N}_{n-1}^T \, d\Omega \\ &= \sum_{p=1}^{3} \sum_{g=1}^{n_g} \rho c \boldsymbol{N}_n(x_g^{(p)}) \boldsymbol{N}_{n-1}^T(x_g^{(p)}) w_g \Omega^{(p)}. \end{aligned} \tag{39}$$

where $\Omega^{(p)}$ is the area of the sub-region p. Then, the expression of the elemental contribution $\frac{\partial C^*_{(e)rk}}{\partial T_j}$ to the derivative reads:

$$\begin{aligned} \frac{\partial C^*_{(e)rk}}{\partial T_j} = \sum_{p=1}^{3} \sum_{g=1}^{n_g} \rho c \Bigg[& \frac{\partial N_{n(r)}}{\partial x_g^{(p)}} \frac{\partial x_g^{(p)}}{\partial s} \frac{\partial s}{\partial T_j} N_{n-1(k)} w_g \Omega^{(p)} \\ & + N_{n(r)} \frac{\partial N_{n-1(k)}}{\partial x_g^{(p)}} \frac{\partial x_g^{(p)}}{\partial s} \frac{\partial s}{\partial T_j} w_g \Omega^{(p)} \\ & + \frac{\partial N_{n(r)}}{\partial x_a} \frac{\partial x_a}{\partial s} \frac{\partial s}{\partial T_j} N_{n-1(k)} w_g \Omega^{(p)} \\ & + N_{n(r)} N_{n-1(k)} w_g \frac{\partial \Omega^{(p)}}{\partial s} \frac{\partial s}{\partial T_j} \Bigg]. \end{aligned} \tag{40}$$

The definition of x_a is given by Eq. (33). The first two terms in Eq. (40) arise from the evaluation dependency, the third term arises from the enrichment dependency and the fourth term arises from the integration region dependency. Computation of the terms $\frac{\partial x_g^{(p)}}{\partial s}$, $\frac{\partial x_a}{\partial s}$ and $\frac{\partial \Omega^{(p)}}{\partial s}$ are straightforward

$$\begin{aligned} \frac{\partial x_g^{(1)}}{\partial s} &= 0 & & & \frac{\partial \Omega^{(1)}}{\partial s} &= 0 \\ \frac{\partial x_g^{(2)}}{\partial s} &= \xi_2 h & \frac{\partial x_a}{\partial s} &= h & \frac{\partial \Omega^{(2)}}{\partial s} &= h \\ \frac{\partial x_g^{(3)}}{\partial s} &= (1-\xi_3) h & & & \frac{\partial \Omega^{(3)}}{\partial s} &= -h \end{aligned} \tag{41}$$

where $\xi_i, i = 1, 2, 3$ are the natural coordinates for each integration region.

The computation of the derivative $\frac{\partial s}{\partial T_j}$ is more cumbersome and is presented in the following paragraphs. This derivative expresses the core of the idea being exposed; it represents how the interface position varies in response to perturbations of the degrees of freedom $\boldsymbol{T}$.

The following preliminary results are needed

$$\frac{\partial E}{\partial x} = \begin{cases} -\dfrac{1}{\phi_1} & x \le x_a \\ -\dfrac{1}{\phi_2} & x > x_a \end{cases} \tag{42}$$

$$\frac{\partial E}{\partial x_a} = \begin{cases} \dfrac{\phi_1 - \phi}{\phi_1^2} & x \le x_a \\ \dfrac{\phi_2 - \phi}{\phi_2^2} & x > x_a \end{cases} \tag{43}$$

$$\frac{\partial E}{\partial s} = \begin{cases} h\dfrac{\phi_1 - \phi}{\phi_1^2} & x \le x_a \\ h\dfrac{\phi_2 - \phi}{\phi_2^2} & x > x_a \end{cases} \tag{44}$$

$$\frac{\partial E}{\partial s} + h\frac{\partial E}{\partial x} = \begin{cases} h\dfrac{\phi_1 - \phi}{\phi_1^2} - \dfrac{h}{\phi_1} = -\dfrac{h\phi}{\phi_1^2} & x \le x_a \\ h\dfrac{\phi_2 - \phi}{\phi_2^2} - \dfrac{h}{\phi_2} = -\dfrac{h\phi}{\phi_2^2} & x > x_a \end{cases} \tag{45}$$

Author's personal copy

The dependence of the temperature field on the position of the interface and on the degrees of freedom $\boldsymbol{T}$, was not explicitly specified in Eq. (35). Making these dependencies explicit and denoting T^h by T to simplify notation, we obtain

$$T(\boldsymbol{T}, x, s) = \sum_i N_i(x) T_i + E(x, s) a. \tag{46}$$

Considering the constraint given by Eq. (6), the temperature at the interface is

$$T(\boldsymbol{T}, x_a, s) = \sum_i N_i(x_a) T_i + a = T_m. \tag{47}$$

Linearising the increment of T, we obtain

$$dT = \frac{\partial T}{\partial \boldsymbol{T}} d\boldsymbol{T} + \frac{\partial T}{\partial x} dx + \frac{\partial T}{\partial s} ds. \tag{48}$$

Considering that the temperature at the interface should be equal to the melting temperature, we obtain

$$dT = \frac{\partial T}{\partial \boldsymbol{T}}\Big|_{x=x_a} d\boldsymbol{T} + \frac{\partial T}{\partial x}\Big|_{x=x_a} dx + \frac{\partial T}{\partial s}\Big|_{x=x_a} ds = 0. \tag{49}$$

Noting from Eq. (33) that $\frac{\partial x}{\partial s}\Big|_{x=x_a} = h$, we obtain

$$\frac{\partial T}{\partial \boldsymbol{T}}\Big|_{x=x_a} d\boldsymbol{T} + \left(h\frac{\partial T}{\partial x} + \frac{\partial T}{\partial s}\right)\Big|_{x=x_a} ds = 0. \tag{50}$$

Therefore, the partial derivative of s with respect to the generalised degrees of freedom $\boldsymbol{T}$ is

$$\frac{\partial s}{\partial \boldsymbol{T}} = -\left(\left(h\frac{\partial T}{\partial x} + \frac{\partial T}{\partial s}\right)\Big|_{x=x_a}\right)^{-1} \frac{\partial T}{\partial \boldsymbol{T}}\Big|_{x=x_a}. \tag{51}$$

The denominator in the Eq. (51) is computed as follows

$$h\frac{\partial T}{\partial x} + \frac{\partial T}{\partial s} = \sum_{i=1}^{2} h\frac{\partial N_i}{\partial x} T_i + \left(\frac{\partial E}{\partial s} + h\frac{\partial E}{\partial x}\right) a, \tag{52}$$

evaluating (52) at the interface $x = x_a$ becomes

$$\left(h\frac{\partial T}{\partial x} + \frac{\partial T}{\partial s}\right)\Big|_{x=x_a} = \sum_{i=1}^{2} h\frac{\partial N_i}{\partial x}(x_a)\, T_i. \tag{53}$$

By replacing the last result (53) into Eq. (51), and by evaluating $\frac{\partial T}{\partial \boldsymbol{T}}\Big|_{x=x_a}$ from Eq. (47), we obtain finally

$$\frac{\partial s}{\partial \boldsymbol{T}} = -\left(\sum_{i=1}^{2} h\frac{\partial N_i}{\partial x}(x_a)\, T_i\right)^{-1} \begin{bmatrix} N_1(x_a) \\ N_2(x_a) \\ 1 \end{bmatrix}. \tag{54}$$

3.6.4 Temperature dependent thermophysical properties.

If we consider problems where the thermophysical properties depend on temperature, new contributions to the tangent matrix arise. These contributions to the elemental level, denoted by $\boldsymbol{\Upsilon}_e$, are given by

$$\boldsymbol{\Upsilon}_e = \sum_{p=1}^{3}\sum_{g=1}^{n_g}\Bigg[\rho \boldsymbol{N}_{n-1}^T \boldsymbol{T}_{n-1} w_g \Omega^{(p)} \boldsymbol{N}_n \frac{\partial c_n}{\partial \boldsymbol{T}}^T + \rho \boldsymbol{N}_n^T \boldsymbol{T} w_g \Omega^{(p)} \boldsymbol{N}_n \frac{\partial c_n}{\partial \boldsymbol{T}}^T + \nabla \boldsymbol{N}_n^T \boldsymbol{T} w_g \Omega^{(p)} \nabla \boldsymbol{N}_n \frac{\partial k_n}{\partial \boldsymbol{T}}^T\Bigg]. \tag{55}$$

The variation of the thermophysical property being considered with respect to $\boldsymbol{T}$ is calculated following the same procedure described before. As an example, we present the computation of the term $\frac{\partial c_n}{\partial \boldsymbol{T}}$. Considering that

$$\frac{\partial c_n(T)}{\partial \boldsymbol{T}} = \frac{\partial c_n(T)}{\partial T}\frac{\partial T}{\partial T_j}\boldsymbol{e}_j \tag{56}$$

we need to calculate the derivative $\frac{\partial T}{\partial \boldsymbol{T}}$ with the specific derivative $\frac{\partial c_n}{\partial T}$ for each considered material.

Taking the increment of the temperature field given by Eq. (46), we have

$$\begin{aligned} &T(\boldsymbol{T} + d\boldsymbol{T}, x + dx, s + ds) \\ &= N_i(x + dx)[T_i + dT_i] + E(x + dx, s + ds)[a + da] \\ &\simeq \left[N_i(x) + \frac{\partial N_i}{\partial x} dx\right][T_i + dT_i] \\ &\quad + \left[E(x, s) + \frac{\partial E}{\partial x} dx + \frac{\partial E}{\partial s} ds\right][a + da] \end{aligned} \tag{57}$$

where N_i and E have been linearised. Considering that the differentials dx and ds are given by

$$dx = \frac{\partial x}{\partial s} ds \qquad ds = \frac{\partial s}{\partial T_j} dT_j + \frac{\partial s}{\partial a} da \tag{58}$$

and ignoring the higher order terms, we obtain

$$\begin{aligned} &T(\boldsymbol{T} + d\boldsymbol{T}, x + dx, s + ds) \\ &= T(\boldsymbol{T}, x, s) + \left[N_j + \frac{\partial N_i}{\partial x}\frac{\partial x}{\partial s}\frac{\partial s}{\partial T_j} T_i + \frac{\partial E}{\partial x}\frac{\partial x}{\partial s}\frac{\partial s}{\partial T_j} a \right. \\ &\quad \left. + \frac{\partial E}{\partial s}\frac{\partial s}{\partial T_j} a\right] dT_j + \left[E + \frac{\partial N_i}{\partial x}\frac{\partial x}{\partial s}\frac{\partial s}{\partial a} T_i \right. \\ &\quad \left. + \frac{\partial E}{\partial x}\frac{\partial x}{\partial s}\frac{\partial s}{\partial a} a + \frac{\partial E}{\partial s}\frac{\partial s}{\partial a} a\right] da \end{aligned} \tag{59}$$

Therefore, the partial derivative of T with respect to the generalised degrees of freedom $\boldsymbol{T}$ is

$$\frac{\partial T}{\partial \boldsymbol{T}} = \boldsymbol{N} + \left(\frac{\partial \boldsymbol{N}}{\partial x} \cdot \boldsymbol{T}\frac{\partial x}{\partial s} + a\frac{\partial E}{\partial s}\right)\frac{\partial s}{\partial \boldsymbol{T}} \tag{60}$$

3.6.5 Algorithmic implementation

Determination of when an element needs to be enriched follows an heuristic approach. The latent heat terms given by Eqs. (25) and (26) are sources of high nonlinearity and this issue must be considered for implementation.

The determination of the integration region for the latent heat vector, Eq. (25), is presented as an example for the one

Author's personal copy

Algorithm 1 Integration region

```
1  Tmax = max(Tj(1:2));
2  Tmin = min(Tj(1:2));
3  solid = false; %if the element is solid,
4                 %then solid=true.
5                 %Otherwise, solid=false
6  %the element is full solid
7  if (Tmax < Tm & abs(Tj(3))<minT3)
8      xL = [x(2);x(2)];
9      solid = true;
10 elseif (Tmin > Tm & abs(Tj(3))<minT3)
11     %the element is full liquid
12     xL=x;
13 else
14     %parameter s determination
15     s = parameterS(Tj,Tm);
16     if (s>=1|s<=0) | ((s<minS | s>(1-minS))
17                          & abs(Tj(3))<minT3)
18         if(Tmax < Tm)
19             solid = true;
20         elseif (Tmin > Tm)
21             solid = false;
22         else
23             diffT = Tj-Tm;
24             index = max(abs(diffT(1:2)));
25             if(sign(diffT(index))==-1)
26                 solid = true;
27             else
28                 solid = false;
29             end
30         end
31         xL = x;
32         if solid
33             xL = [x(2);x(2)];
34         end
35     else
36         ifpos = [elementNumber,s];
37         %the element is enriched
38         eAct = true;
39         %phase change element, x1 is solid
40         if(Tj(2)>Tj(1))
41             xL = [ x(1)+s*h; x(2)];
42         else
43             %phase change element
44             %x1 is liquid
45             xL = [ x(1); x(1)+s*h];
46         end
47     end
48 end
```

dimensional case (Algorithm 1). The degrees of freedom of the element are given by the vector `Tj`=[T_1, T_2, a], the integration region is denoted by variable `xL`, and `x` represents the whole element domain.

The element is processed as a full solid element if the nodal temperatures are below the melting temperature, and if the absolute value of the enrichment degree of freedom, denoted by a, is below a certain threshold `minT3` (an element in which a > `minT3` still has latent heat inside and cannot be considered as a full solid element). The same applies for the determination of the liquid state, but this time the nodal temperatures are above the melting temperature.

If the element is neither liquid nor solid, the element is supposed to be in a phase change state, i.e., one portion of the element is liquid and the other is solid. In this case, the interface position parameter s is determined using Eq. (38).

If parameter s is admissible, i.e., if s falls within the range (0, 1), then the element is enriched (lines 36–46) and the integration region `xL` is computed. The number identifying the element being enriched and the local interface position parameter s are tracked by the variable `ifpos`.

When the element is supposed to be in phase change state, it could be possible for local parameter s to exceed the range (0, 1) when it is computed. In this situation, to avoid the divergence of the Newton–Raphson scheme the element is not processed as a phase change element, instead it is considered liquid or solid. In this context to determine the element state, two cases must be considered:

- It could happen that the nodal temperatures are both below or above the melting temperature, but with the absolute value of the parameter a being greater than the threshold `minT3`. In this case, the element is considered liquid or solid based on the nodal temperatures values (lines 18–22).
- If the nodal temperatures are not either all below or all above the melting temperature, the element state is computed based on the relative value of the nodal temperatures with respect to the melting temperature. That is, we determine the maximum relative temperature taking into account absolute values. Then, if the sign associated to that maximum is negative, the element is processed as solid. If this is not the case, it is considered liquid. This issue is addressed in lines 22–30 of the code.

Finally, if the interface is located too close to an element node position and the enrichment parameter is too low, the Newton–Raphson scheme can lead to divergence (note that in this case the element is almost fully solid or fully liquid). In order to avoid this situation, whenever the parameter s is below the threshold `minS` or above the threshold 1-`minS`, and the absolute value of the enrichment parameter a is below the threshold `minT3`, the element is not enriched (second part of the conditional, line 16 of the code).

The threshold values are determined as follows. The threshold `minT3` for the enrichment a is given by

$$\texttt{minT3} = \text{tol}_T T_c n^{1/d} \tag{61}$$

where T_c is a characteristic temperature of the problem, n is the number of elements, d is the number of spatial dimensions and tol_T is a tolerance set equal to 10^{-5}. The threshold `minS` for the parameter s is set equal to 5×10^{-5}.

Author's personal copy

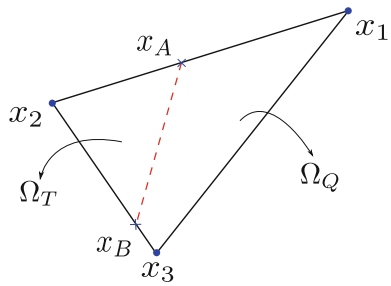

Fig. 2 Example of a two-dimensional phase change element

3.7 Extension to two dimensions

A discussion on the two dimensional extension of the discrete formulation is presented. Its implementation is left as future work. The enrichment shape functions E for the two dimensional case can be generated as described by Soghrati et al. [34].

Let us consider a phase change element as displayed in Fig. 2. For the current analysis, suppose that $T_2 > T_m$, $T_1 < T_m$ and $T_3 < T_m$; then, the interface intersects the sides l_{12} and l_{23} of the element as shown in the figure. The intersection points of the interface with the boundary are denoted by $\boldsymbol{x}_A$ and $\boldsymbol{x}_B$.

We divide the element in its *bilinear* subregion Ω_Q and its *linear* subregion Ω_T. Then, two enrichment functions corresponding to points $\boldsymbol{x}_A, \boldsymbol{x}_B$ can be defined as

$$E_I(\boldsymbol{x}) = \begin{cases} Q_I(\boldsymbol{x}) & \boldsymbol{x} \in \Omega_Q \\ N_I(\boldsymbol{x}) & \boldsymbol{x} \in \Omega_T \end{cases}, \qquad I = A, B. \tag{62}$$

The temperature interpolation inside an enriched element is then given as:

$$T^h(\boldsymbol{x}, s_A, s_B) = \sum_i N_i(\boldsymbol{x}) T_i + E_A(\boldsymbol{x}, s_A) a + E_B(\boldsymbol{x}, s_B) b. \tag{63}$$

where $N_i(\boldsymbol{x})$ are the standard linear shape functions, and where parameters s_A, s_B express the position of points $\boldsymbol{x}_A, \boldsymbol{x}_B$ in terms of the nodal positions of the element:

$$\boldsymbol{x}_A = \boldsymbol{x}_1 + s_A(\boldsymbol{x}_2 - \boldsymbol{x}_1) \tag{64}$$

$$\boldsymbol{x}_B = \boldsymbol{x}_2 + s_B(\boldsymbol{x}_3 - \boldsymbol{x}_2). \tag{65}$$

Note that, from the definition of the enrichment function, the interface is straight inside a phase change element. To compute (62), we need to know positions $\boldsymbol{x}_A$ and $\boldsymbol{x}_B$.

The value of s_A, s_B will be determined from the requirement that the temperature at the interface should be equal to the melting temperature T_m, similarly to what we made in the one dimensional case. Then, we write

$$T_m = T_1 N_1^B(s_A) + T_2 N_2^B(s_A) + a, \tag{66}$$

where $N_1^B(s_A)$ and $N_2^B(s_A)$ are the restrictions of the shape functions $N_1(\boldsymbol{x})$ and $N_2(\boldsymbol{x})$ to the boundary l_{12}, and a is the amplitude of the enrichment function $E_A(\boldsymbol{x})$.

Following the same procedure used for the one dimensional case, we can show that:

$$s_A = \frac{T_m - T_1 - a}{T_2 - T_1}. \tag{67}$$

The expression for s_B is obtained in a similar form.

4 Numerical examples

The method was tested in a series of challenging one dimensional problems, i.e. problems with extreme values of temperature gradient discontinuity and problems with initial temperatures close to the melting temperature. The obtained results were compared with analytic solutions and with the results obtained from a fixed mesh numerical scheme, for which the temperature gradient discontinuity was not considered. Also, results for the first problem are compared against results obtained with an existing enriched formulation.

In the following examples, we use the normalised residual norm to ascertain the convergence of the Newton–Raphson scheme. This normalised residual norm is given by

$$\frac{\|\boldsymbol{\Pi}\|}{\|\boldsymbol{F_r}\| + \|\boldsymbol{F_c}\| + \|\boldsymbol{F_k}\|}, \tag{68}$$

where $\| \cdot \|$ denotes the L_2 norm of $\cdot$ and

$$\boldsymbol{F_r} = \frac{\boldsymbol{L}_n - \boldsymbol{L}_{n-1}}{\Delta t} + \boldsymbol{F} - \boldsymbol{Q} \tag{69}$$

$$\boldsymbol{F_c} = \frac{\boldsymbol{C}\boldsymbol{T}_n}{\Delta t} - \frac{\boldsymbol{C}^*\boldsymbol{T}_{n-1}}{\Delta t} \tag{70}$$

$$\boldsymbol{F_k} = \boldsymbol{K}\boldsymbol{T}_n. \tag{71}$$

4.1 Problem I: Dirichlet/Dirichlet boundary conditions

In this problem we show the performance of the proposed enriched formulation, comparing results with those obtained by Merle and Dolbow [27]. A solution obtained using the method without enrichment by Fachinotti et al. [14] is shown. All solutions are compared to the exact solution, computed for a semiinfinite bar. A similar problem was also treated in reference [26].

The problem consists in the freezing of a long slab that was initially at temperature T_0 above the melting temperature T_m and is suddenly cooled by imposing a constant temperature $T_1 < T_m$ to the slab end $x = 0$. The temperature at the slab end $x = L$ is held at $T_0 > T_m$, where L is the slab length. The parameters of the problem are given in Table 1. The Stefan number St_s for this problem is given by

Author's personal copy

Table 1 Problem I parameters

$\mathcal{L}$	c_s	c_l	k_s	k_l
19.2 J/kg	0.49 J/ °C/kg	0.62 J/ °C/kg	9.6×10^{-3} W/ °C/cm	6.9×10^{-3} W/ °C/cm
ρ	T_m	T_1	L	T_0
1 kg/cm^3	0 °C	−10 °C	10 cm	4 °C

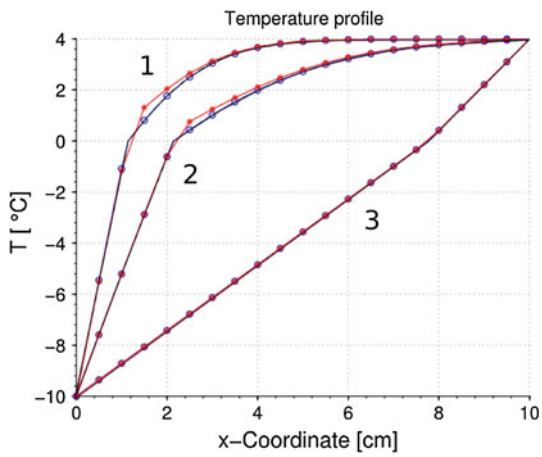

Fig. 3 Temperature profile at different time instants: *1* $t = 180$ s, *2* $t = 360$ s, and *3* steady-state solution. *Solid line* Merle and Dolbow's solution, *dashed line* exact solution, *asterisks* solution without enrichment, and *circles* solution with the proposed enrichment. Merle and Dolbow's, exact and the solution with the proposed method are all coincident

Table 2 Problem I: normalised residual norm for selected time steps for the proposed method

Iter.	$t = 12.76$ s	$t = 127.6$ s	$t = 446.6$ s	$t = 1339.8$ s
0	0.9995	0.6973	0.6677	0.6684
1	0.8778	0.0616	0.0236	0.0266
2	0.8820	0.0001	0.0002	0.0003
3	0.6078	2.7e−9	1.1e−8	1.7e−8
4	0.3627	1.2e−15	4.3e−15	1.1e−14
⋮	⋮			
6	0.0035			
7	3.7e−6			
8	2.5e−12			

$$\mathrm{St}_s = \frac{c_s(T_m - T_1)}{\mathcal{L}} = 0.255. \tag{72}$$

Twenty equally spaced elements and a time step of 12.76s are used to model this problem. The computed solution is shown in Fig. 3 for different time instants. Perfect agreement with the results obtained by Merle and Dolbow [27] and with the exact solution can be observed. The solution obtained with the method without enrichment displays a small error near the interface between solid and liquid zones.

The proposed numerical scheme took an average of 2.55 iterations per time to get the solution, with a maximum of 8 iterations in the first time step. On the other hand, Merle and Dolbow reported less than 15 iterations to get a solution with their XFEM method. In Table 2 the evolution of the normalised residual norm for a number of representative time steps is given, showing quadratic convergence in all cases.

4.2 Problem II: Dirichlet/Dirichlet boundary conditions with a low Stefan number

Again, the freezing of a long slab is analyzed; nevertheless, a much larger value of latent heat is now used. In this way, the behaviour of the proposed numerical formulation with very low Stefan numbers is studied. The slab is initially at temperature T_0 above the melting temperature T_m and is suddenly cooled by imposing a constant temperature $T_1 < T_m$ to the slab end $x = 0$. The temperature at the slab end $x = L$ is held at $T_0 > T_m$, where L is the slab length. The parameters of the problem are given in Table 3. The Stefan number St_s for this problem is given by

$$\mathrm{St}_s = \frac{c_s(T_m - T_1)}{\mathcal{L}} = 0.025 \tag{73}$$

Sixteen equally spaced elements and a time step of 18s are used to model this problem. The computed solution is shown in Fig. 4 for different time instants and is compared with the analytic solution for a semi-infinite medium [37] showing almost perfect agreement. Additionally, the solution obtained with the formulation without enrichment proposed by Fachinotti et al. [14] is shown in dashed lines. The solution without enrichment presents spurious oscillations and, in certain time instants, is quite different from the analytic solution.

Figure 5 displays the interface evolution over time. Again, the current method shows almost perfect agreement with the analytical solution, while the formulation without enrichment differs from the analytic solution.

A quadratic convergence rate was observed in all time steps. The mean number of iterations per time step was 3.71, and the maximum number of iterations at a given time step was 12. These values are similar to those for the fixed mesh technique, which required 3.32 iterations per time step, with a maximum of 7 iterations.

Author's personal copy

Table 3 Problem II parameters

$\mathcal{L}$	c_s	c_l	k_s	k_l
190.26 J/kg	0.49 J/ °C/kg	0.62 J/ °C/kg	9.6×10^{-3} W/ °C/m	6.9×10^{-3} W/ °C/m
ρ	T_m	T_1	L	T_0
1 kg/m^3	0 °C	−10 °C	10 m	4 °C

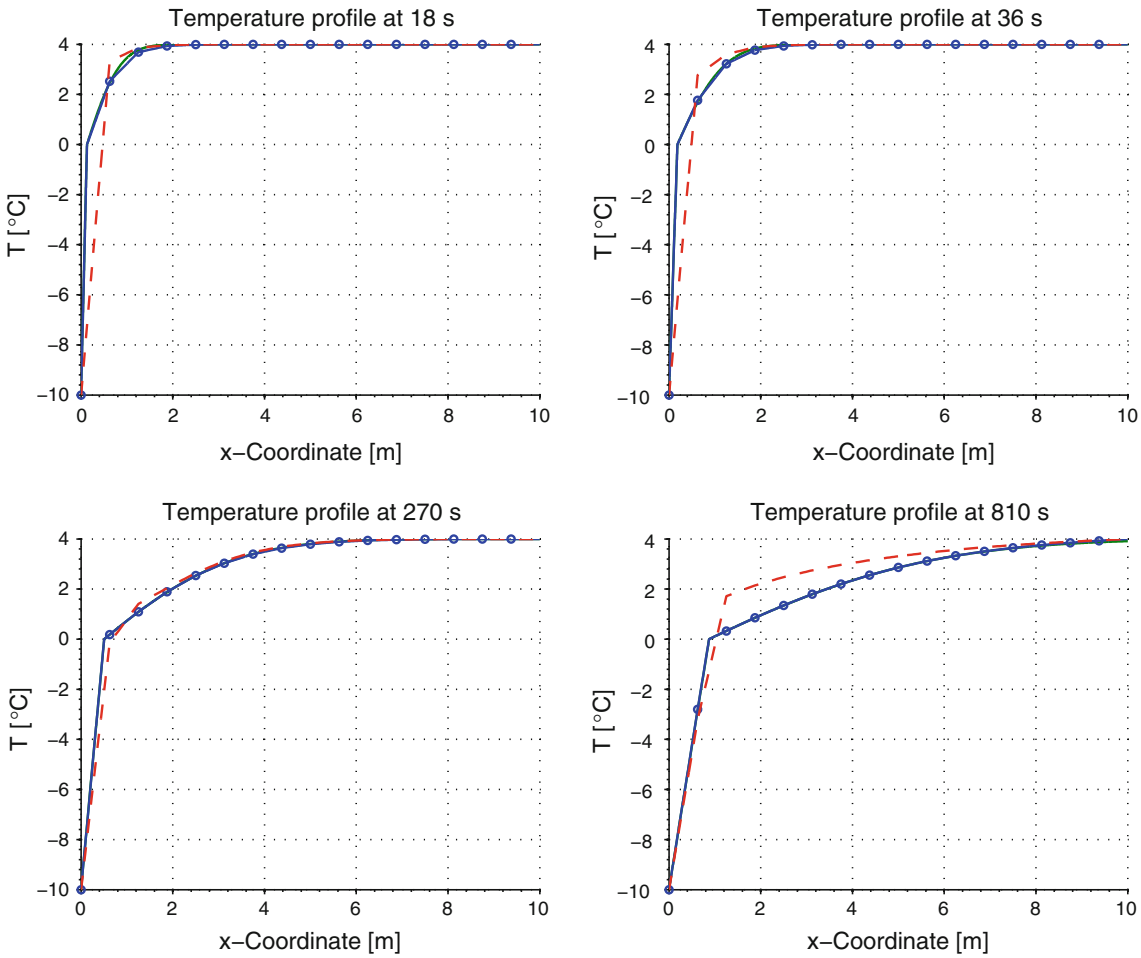

Fig. 4 Solution of problem II at different time steps. *Solid line* the exact solution, *dashed line* approximate solution without enrichment, *solid line with circles* approximate solution obtained with the proposed method

In Table 4 the evolution of the residual for a number of representative time steps can be observed. The maximum number of iterations is attained at the first time step ($t = 18$ s) because at the initial time ($t = 0$ s), the interface is located too close to the first node to accurately represent the initial condition (a heaviside at $x = 0$). It should be noted that the element's capability to represent this type of temperature distribution causes the observed accurate results. If the initial position of the interface is placed farther from $x = 0$, the number of iterations will be smaller, but the approximation to the exact solution of the problem will be less accurate. The errors with the method without enrichment are due, in part, to the impossibility of this formulation of representing this initial condition.

Figure 6 provides the temperature evolution at $x = 0.625$ m for meshes of 16, 32, 64 and 128 equally spaced elements. In all cases a time step of 18s was used. Results for the method without enrichment are shown for all meshes. We can see that an error appears even for the mesh with 128 elements. The proposed method of enrichment, gives results which are almost coincident with the exact results, for a mesh of only 16 elements. Computations with 64 elements are completely coincident with the 16 elements results.

Author's personal copy

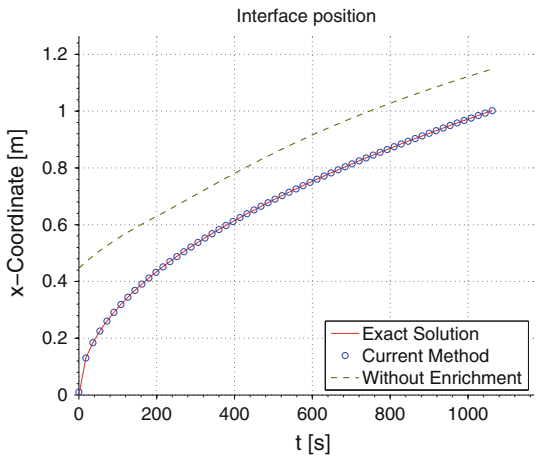

Fig. 5 Interface position with exact and approximate values

Table 4 Problem II: normalised residual norm evolution for the proposed formulation at selected time steps

Iter.	$t=18\,\mathrm{s}$	$t=126\,\mathrm{s}$	$t=234\,\mathrm{s}$	$t=324\,\mathrm{s}$
0	0.9997	0.8926	0.8453	0.8208
1	0.9903	0.0159	0.0097	0.0076
2	0.9770	0.0001	4.7e−5	1.7e−5
3	0.9575	1.7e−9	3.7e−10	1.1e−10
4	0.9267	1.1e−15		
⋮	⋮			
10	0.0006			
11	5.8e−7			
12	4.8e−13			

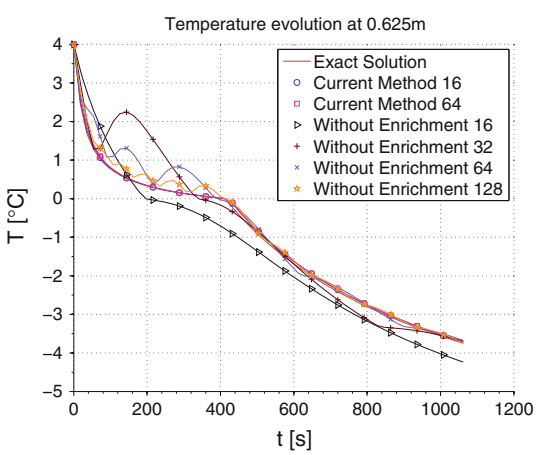

Fig. 6 Temperature evolution. Exact and approximate values for different number of equally spaced elements

The method without enrichment using 32 equally spaced elements displays spurious oscillations of increasing amplitude with respect to the mesh with 16 elements. These oscillations are observed in all computations with the method without enrichment. This fact can hinder its use for the estimation of temperature time rates which are necessary, i.e. for the computation of microstructure.

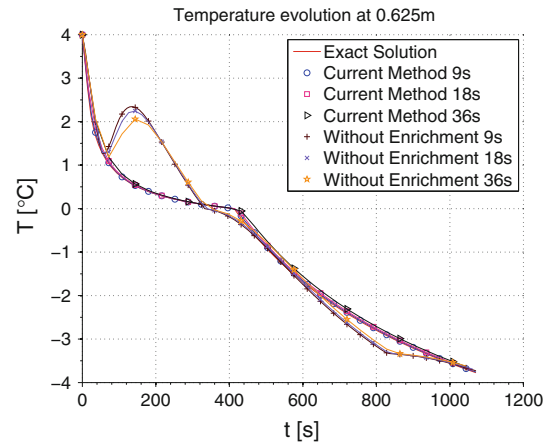

Fig. 7 Temperature evolution. Exact and approximate values for different time steps

Table 5 Parameters of problem III

$\mathcal{L}$	c	k	ρ
190.26 J/kg	1 J/ °C/kg	1.08 W/ °C/m	1 kg/m^3
T_m	T_1	L	T_0
−0.1 °C	45 °C	4 m	−4 °C

Figure 7 provides the temperature evolution at $x = 0.625\,\mathrm{m}$ for time steps 9, 18 and 36 s, with a mesh of 32 equally spaced elements. The conclusions obtained for this experiment are similar to those obtained for the previous experiment. Our method gives accurate results without temporal oscillations, whereas the method without enrichment present spurious oscillations.

4.3 Problem III: Dirichlet/Neumann boundary conditions

Here, we study the melting of a long slab initially at temperature T_0 below the melting temperature T_m that is suddenly heated by imposing a constant temperature $T_1 >> T_m$ at the slab end $x = 0$. The slab end $x = L$ is insulated, where L is the slab length. The analytic solution for a semi-infinite medium associated with this problem can be found in [1].

The thermophysical parameters are considered constant and equal in both phases, such that $c = c_s = c_l$ and $k = k_s = k_l$. The problem parameters are given in Table 5.

Twelve equally spaced elements and a time step of 0.2 s are used to model this problem. The computed solution is shown in Fig. 8 for different time instants and is compared with the analytic solution, showing almost perfect agreement. Additionally, the solution obtained using the formulation without

Author's personal copy

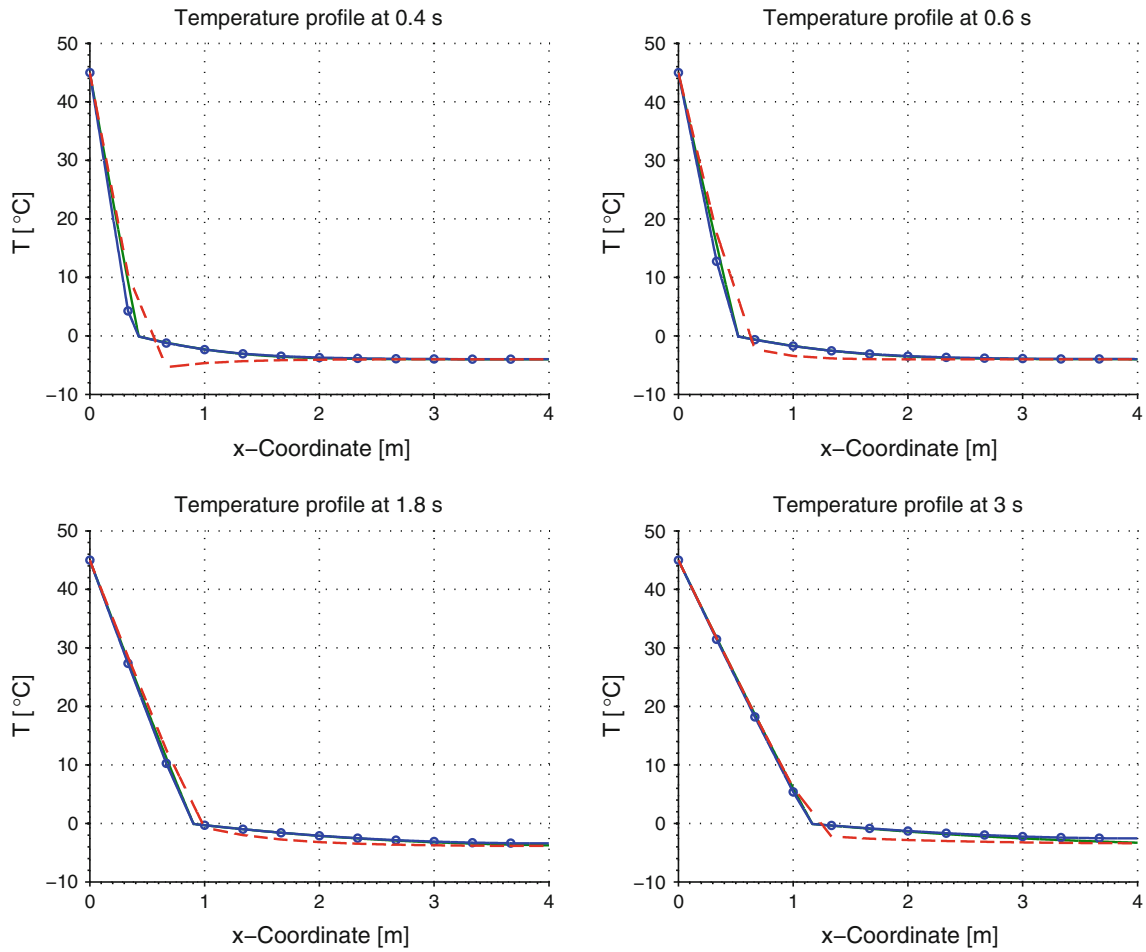

Fig. 8 Solution of problem III at different time steps. The *solid line* is the exact solution. The *dashed line* is the approximate solution without enrichment. The *solid line with circles* is the approximate solution obtained with the proposed method

enrichment, proposed by Fachinotti et al. [14], is shown with dashed lines. The solution without enrichment includes spurious oscillations, and in certain time instants is quite different from the analytic solution.

Figure 9 displays the interface evolution over time. Again, the method with enrichment shows nearly perfect agreement with the analytical solution, while the formulation without enrichment does not. In Fig. 10 the temperature evolution at node 2 ($x = 0.33$ m) is provided. The enriched solution follows the analytic solution quite well, while the solution without enrichment has severe oscillations.

The Stefan number St_l for this problem is given by

$$\mathrm{St}_l = \frac{c_l(T_l - T_m)}{\mathcal{L}} = 0.23704. \tag{74}$$

The computational effort in this problem was important because of the high nonlinearity from our formulation. The mean number of iterations per time step was 12, and the maximum number of iterations at a given time step was 35. These values are much greater than those acquired with the fixed mesh technique, which required 4.95 iterations per time step with a maximum of 8 iterations. Nevertheless, the computed solution showed high accuracy, such that even though the Stefan number was small, the solution was quite close to

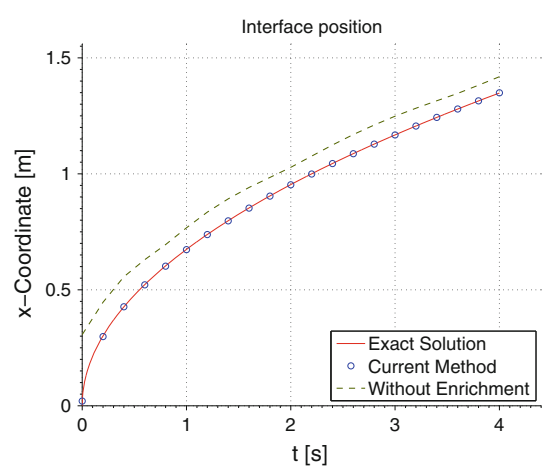

Fig. 9 Interface position with exact and approximate values

Author's personal copy

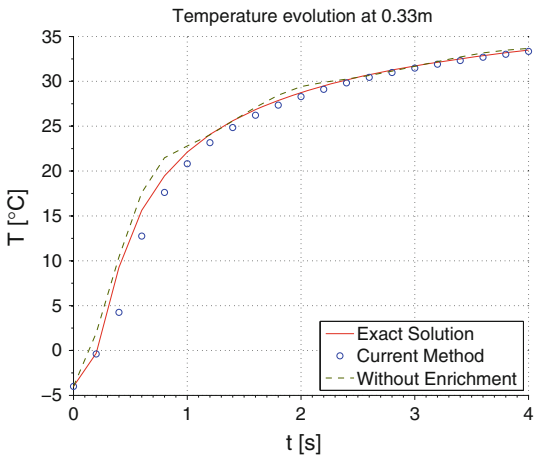

Fig. 10 Temperature evolution with exact and approximate values

Fig. 11 Square cylinder produced by SMD

the analytical solution and did not have spurious oscillations (these oscillations are undesirable, e.g., when computing the microstructure, which depends on the temperature history and on the temperature rates).

4.4 Problem IV: simplified tig-wash problem

This problem studies the behaviour of the proposed method under the presence of a moving heat source and with typical thermal dependent material properties. Figure 11 shows a sample square tube part made by SMD of Ti–6Al–4V alloy that was built by deposing material with a welding tig robot [2]. A simplified one dimensional model of this part is analysed during the "tig-wash" procedure, where the part is heated using the welding torch without deposing the material.

The dimensions of the cross-section of the bead are $d_1 = 9.83$mm wide and $d_2 = 70$mm high. Initially the bead is at room temperature $T_e = 299$K. Suddenly the heat source starts to heat the body from the top, traveling at a known velocity. At the same time, the part is cooled through the top and side walls by air convection and radiation (Robin boundary conditions are assumed for combined convection and radiation). The base of the bead is considered to remain at constant temperature T_e.

Table 6 Parameters of problem IV

$\mathcal{L}$	T_m	ρ	Q	Torch speed
292,600 J/kg	1,905 K	4,430 kg/m^3	1,512 J	5 mm/s
c_r	c_f	f_f	f_r	T_f
10 mm	2.5 mm	0.4	1.6	299 K

We assume that heat conduction along the longitudinal and transversal directions can be neglected to build a simplified one-dimensional model. The heat source can be described using a simplification of the Goldak heat source [18], which is obtained as follows for the one dimensional case [13]

$$Q_s(t) = \frac{\sqrt{3}Q}{\sqrt{\pi}d_1} \begin{cases} \frac{f_f}{c_f} \exp\left(-3\frac{z(t)^2}{c_f^2}\right) & \text{if } z(t) \leq 0 \\ \frac{f_r}{c_r} \exp\left(-3\frac{z(t)^2}{c_r^2}\right) & \text{if } z(t) > 0 \end{cases} \tag{75}$$

where c_f and c_r are the length parameters associated with the axis of the front and rear semi-ellipsoids, f_f and f_r are the portion of heat distributed in the front and rear semi-ellipsoids, respectively, and Q is the total heat input. The function $z(t)$ gives the variation of position of the heat source relative to the plane containing the cross section of the bead.

The material properties and other parameters of the problem are described in Table 6. The heat capacity c, the thermal conductivity k and the thermal convection / radiation coefficient h_f depend on the temperature and are given by the expressions [2]

$$c\left[\frac{\text{J}}{\text{kgK}}\right] = 0.17919\, T[\text{K}] + 495.20$$

$$k\left[\frac{\text{W}}{\text{mK}}\right] = \begin{cases} 0.0107\, T[\text{K}] + 4.6619 & T \leq 1905\text{K} \\ 0.5733\, T[\text{K}] - 1067.2 & T > 1905\text{K} \end{cases}$$

$$h_f\left[\frac{\text{W}}{\text{m}^2\text{K}}\right] = 0.26\, T[\text{K}] - 55.$$

The variation in time of the total heat input at the considered cross-section $Q_s(t)$ for the proposed parameter values is given in Fig. 12.

Note that the Robin boundary conditions on the side walls are represented in the one dimensional model as a sink. These terms, denoted by $\boldsymbol{\Xi}$, are

$$\boldsymbol{\Xi} = \frac{2}{d_1}\int_{\Omega} h_{f_n} \boldsymbol{N}_n \boldsymbol{N}_n^T \, d\Omega \boldsymbol{T} - \frac{2}{d_1}\int_{\Omega} h_{f_n} \boldsymbol{N}_n T_f \, d\Omega, \tag{76}$$

Author's personal copy

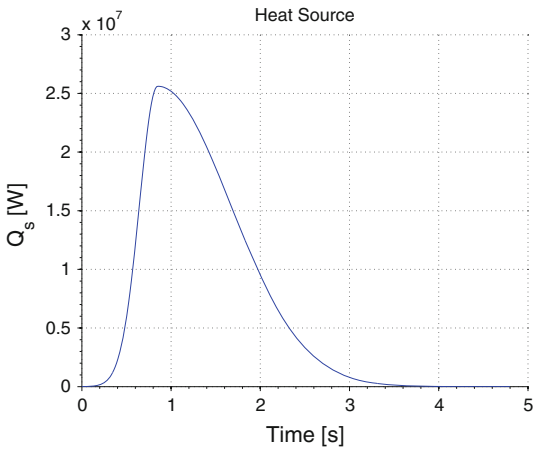

Fig. 12 Heat source variation

with the elemental contribution $\boldsymbol{\Xi}_e$ given by

$$\boldsymbol{\Xi}_e = \frac{2}{d_1}\sum_{p=1}^{3}\sum_{g=1}^{n_g}\Big[h_{f_n}\boldsymbol{N}_n\boldsymbol{N}_n^T w_g \Omega^{(p)}\boldsymbol{T} - h_{f_n}\boldsymbol{N}_n T_f w_g \Omega^{(p)}\Big]. \tag{77}$$

If we consider the temperature dependence of the thermal convection coefficient h_{f_n}, new contributions to the tangent matrix arise, which are given to the elemental level by

$$\boldsymbol{\Upsilon}_e^{h_f} = \frac{2}{d_1}\sum_{p=1}^{3}\sum_{g=1}^{n_g}\Big[\boldsymbol{N}_n^T\boldsymbol{T}_n w_g \Omega^{(p)}\boldsymbol{N}_n \frac{\partial h_{f_n}}{\partial \boldsymbol{T}}^T - T_f w_g \Omega^{(p)}\boldsymbol{N}_n \frac{\partial h_{f_n}}{\partial \boldsymbol{T}}^T\Big]. \tag{78}$$

A time step of 0.015 s and 32 equally spaced elements are used to model this problem. The results obtained after running the simulation are shown in Figs. 13 and 14. In Fig. 14, a non physical variation can be observed in the initial transient due to a thermal shock problem. The maximum number of iterations was 4 iterations with a mean of 2.01 iterations per time step.

The temperature evolution over time at $x = 70$mm is shown in Fig. 15a. To understand the phenomenon observed in this figure, the temperature space profile at $t = 3.279$s is shown in Fig. 15b. This behaviour is physically correct, as it represents the initial solidification of the weld surface with

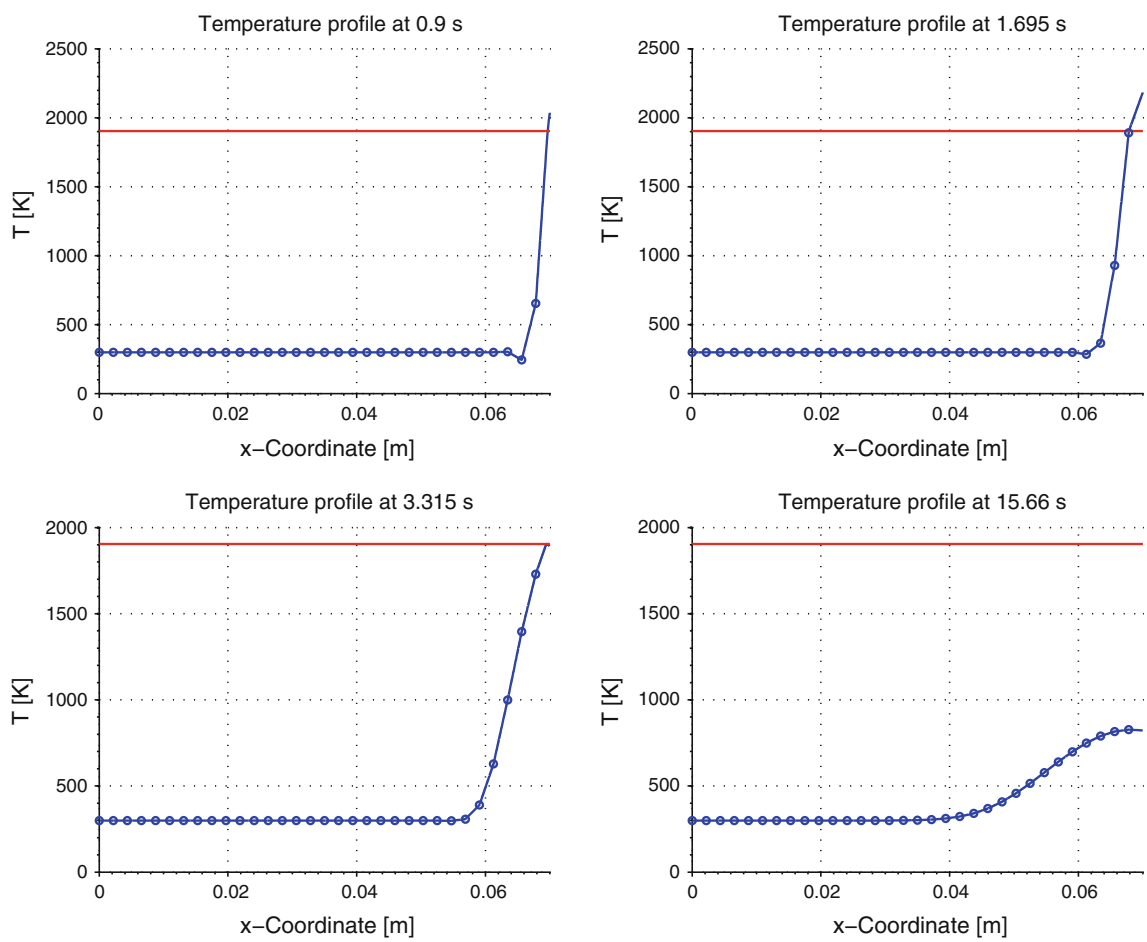

Fig. 13 Temperature profile at different time steps

Author's personal copy

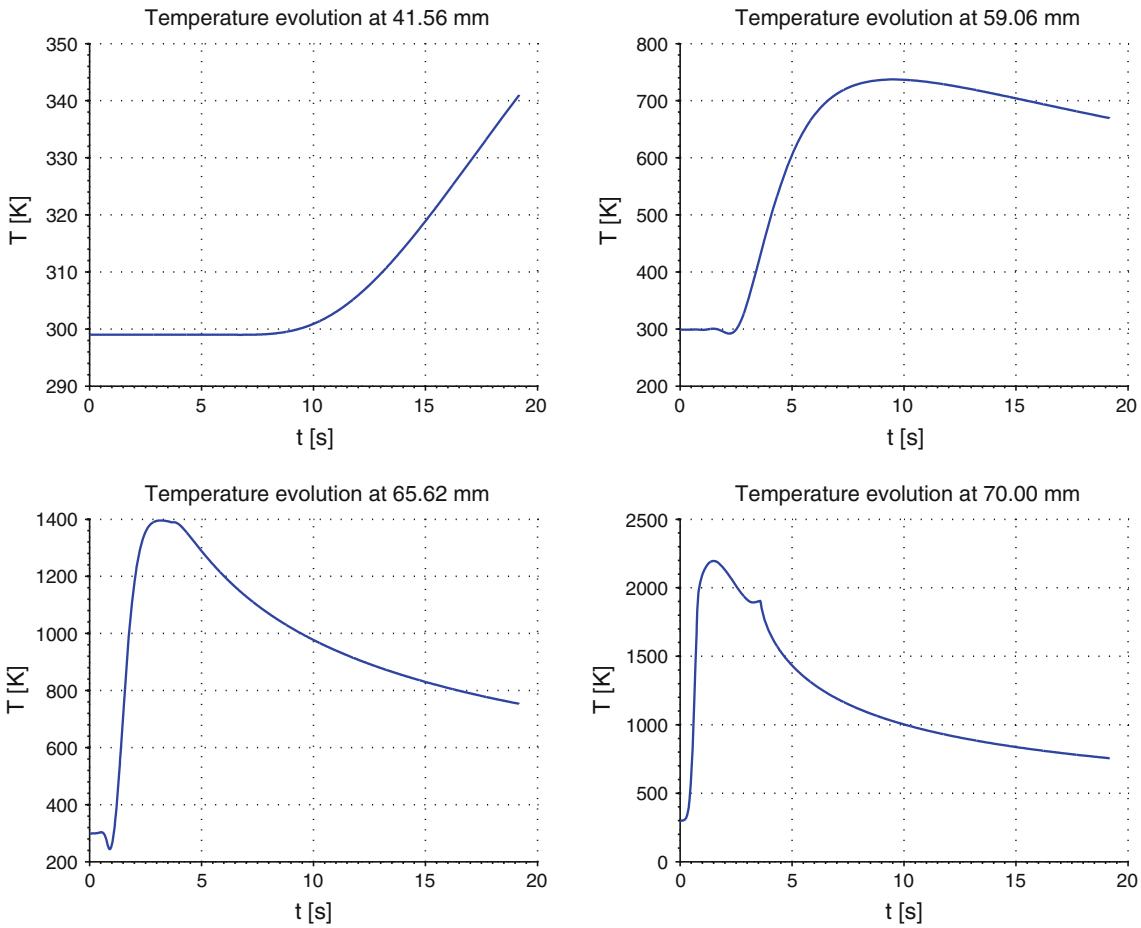

Fig. 14 Temperature evolution at different points

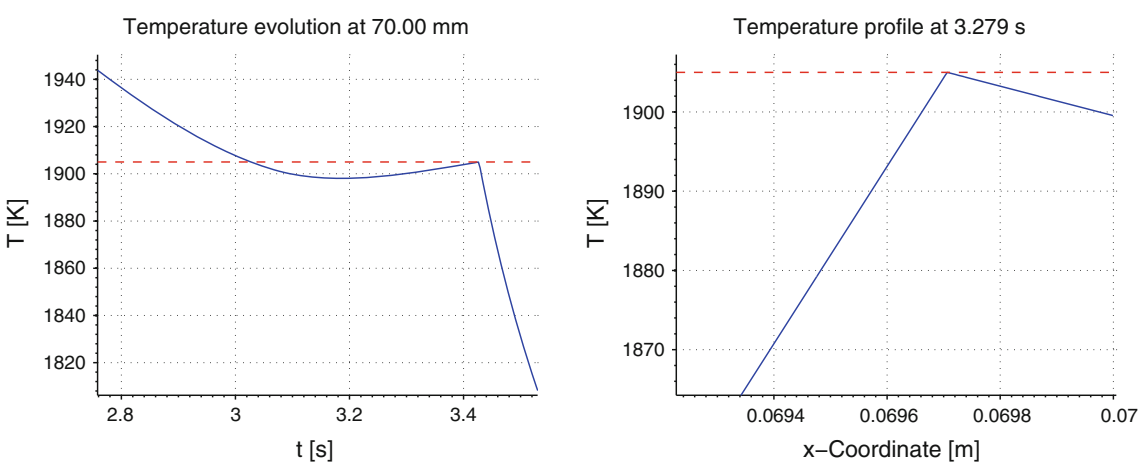

(a) Detail: temperature evolution at 70mm. **(b)** Detail: temperature at 3.279s.

Fig. 15 Details of problem IV (melting temperature is the *dashed line* and temperature evolution is the *solid line*)

Author's personal copy

some liquid inside, which is a typical behaviour observed during the welding processes [22]. To show these details with high resolution a time step of 0.003 s was used to obtain the results.

5 Conclusions

A new approach for solving isothermal phase change problems was presented. The method has the advantages of a fixed mesh method that does not need remeshing to conform to the phase change interface, but also introduces the possibility to represent the discontinuity in the temperature gradient at the solidification front by enriching locally where it is necessary. The proposed method also avoids the use of an auxiliary equation to determine the enrichment position, which is common for level set formulations; instead, this position is determined with a constraint that imposes that the temperature at the phase change boundary must be the melting temperature.

Different test problems were investigated. The proposed method ran these tests giving results that were more accurate than with a formulation without enrichment and without presenting any spurious oscillations. Additionally, a simplified welding problem for a Titanium alloy was presented to study the behaviour of the current method under the influence of a moving heat source and for typical material values. This method is able to handle this type of problem. In future work, the formulation of two and three-dimensional implementations will be considered.

Acknowledgments This study has received financial support from Consejo Nacional de Investigaciones Científicas y Técnicas (CONICET), Universidad Nacional del Litoral (UNL) and Autoridad Regulatoria Nuclear (ARN).

References

1. Alexiades V, Solomon AD (1993) Mathematical modeling of melting and freezing processes. Hemisphere Publishing Corporation, Taylor and Francis Group, Washington
2. Anca A, Fachinotti VD, Escobar-Palafox G, Cardona A (2011) Computational modelling of shaped metal deposition. Int J Numer Methods Eng 85(1):84–106
3. Ausas RF, Buscaglia GC, Idelsohn SR (2011) A new enrichment space for the treatment of discontinuous pressures in multi-fluid flows. Int J Numer Methods Fluids 43:555–575
4. Baines MJ, Hubbard ME, Jimack PK (2005) A moving mesh finite element algorithm for the adaptive solution of time-dependent partial differential equations with moving boundaries. Appl Numer Math 54(3–4):450–469
5. Basombrío F (1997) El problema de dos fases en materiales heterogéneos. aplicaciones. Revista Internacional de Métodos Numéricos para Cálculo y Diseño en Ingeniería 13(3):351–366
6. Beckett G, MacKenzie JA, Robertson ML (2001) A moving mesh finite element method for the solution of two-dimensional stefan problems. J Comput Phys 168(2):500–518
7. Bernauer M, Herzog R (2012) Implementation of an X-FEM solver for the classical two-phase Stefan problem. J Sci Comput 52(2):271–293
8. Celentano D, Oñate E, Oller S (1994) A temperature-based formulation for finite element analysis of generalized phase-change problems. Int J Numer Methods Eng 37(20):3441–3465
9. Chessa J, Smolinski P, Belytschko T (2002) The extended finite element method (XFEM) for solidification problems. Int J Numer Methods Eng 53(8):1959
10. Coppola-Owen AH, Codina R (2005) Improving eulerian two-phase flow finite element approximation with discontinuous gradient pressure shape functions. Int J Numer Methods Fluids 49(12):1287–1304
11. Crivelli LA, Idelsohn SR (1986) A temperature-based finite element solution for phase-change problems. Int J Numer Methods Eng 23(1):99–119
12. Davey K, Mondragon R (2010) A non-physical enthalpy method for the numerical solution of isothermal solidification. Int J Numer Methods Eng 84(2):214–252
13. Fachinotti V, Cardona A, Cosimo A, Baufeld B, Van der Biest O (2010) Evolution of temperature during shaped metal deposition: Finite element predictions vs. observations. Mecánica Computacional 19:4915–4926
14. Fachinotti VD, Cardona A, Huespe AE (1999) A fast convergent and accurate temperature model for phase-change heat conduction. Int J Numer Methods Eng 44(12):1863–1884
15. Fries T (2008) A corrected XFEM approximation without problems in blending elements. Int J Numer Methods Eng 75(5): 503
16. Fries TP, Belytschko T (2010) The extended/generalized finite element method: an overview of the method and its applications. Int J Numer Methods Eng 84(3):253–304
17. Fries TP, Zilian A (2009) On time integration in the XFEM. Int J Numer Methods Eng 79(1):69
18. Goldak J, Chakravarti A, Bibby M (1984) A new finite element model for welding heat sources. Metall Mater Trans B 15:299–305
19. Idelsohn S, Storti M, Crivelli L (1994) Numerical methods in phase-change problems. Arch Comput Methods Eng 1:49–74
20. Ji H, Chopp D, Dolbow JE (2002) A hybrid extended finite element/level set method for modeling phase transformations. Int J Numer Methods Eng 54(8):1209–1233
21. Kelley CT (1999) Iterative methods for optimization. Society for Industrial and Applied Mathematics, Philadelphia
22. Kelly SM (2004) Thermal and microstructure modeling of metal deposition processes with application to Ti–6Al–4V. Ph.D. thesis, Faculty of the Virginia Polytechnic Institute and State University, Blacksburg
23. Koric S, Thomas BG (2006) Efficient thermo-mechanical model for solidification processes. Int J Numer Methods Eng 66(12): 1955–1989
24. Ladevèze P, Simmonds JG (1999) Nonlinear computational structural mechanics: new approaches and non-incremental methods of calculation. Springer, Paris
25. Lindgren L (2007) Computational welding mechanics: thermomechanical and microstructural simulations. Woodhead Publishing, Abington
26. Lynch DR, O'Neill K (1981) Continuously deforming finite elements for the solution of parabolic problems, with and without phase change. Int J Numer Methods Eng 17(1):81–96
27. Merle R, Dolbow J (2002) Solving thermal and phase change problems with the extended finite element method. Comput Mech 28(5):339

Author's personal copy

28. Nallathambi AK, Specht E, Bertram A (2009) Computational aspects of temperature-based finite element technique for the phase-change heat conduction problem. Comput Mater Sci 47(2):332
29. Nigro N, Huespe A, Fachinotti V (2000) Phasewise numerical integration of finite element method applied to solidification processes. Int J Heat Mass Transf 43(7):1053–1066
30. Runnels SR, Carey GF (1991) Finite element simulation of phase change using capacitance methods. Numer Heat Transf B 19(1):13–30
31. Salcudean M, Abdullah Z (1988) On the numerical modelling of heat transfer during solidification processes. Int J Numer Methods Eng 25(2):445–473
32. Sethian JA (1996) Level set methods and fast marching methods. Cambridge University Press, Cambridge
33. Simone A (2007) Partition of unity-based discontinuous finite elements: GFEM, PUFEM, XFEM. Revue Européenne de Génie Civil 11(7-8):1045
34. Soghrati S, Aragón AM, Armando Duarte C, Geubelle PH (2012) An interface-enriched generalized FEM for problems with discontinuous gradient fields. Int J Numer Methods Eng 89(8):991–1008
35. Storti M, Crivelli LA, Idelsohn SR (1987) Making curved interfaces straight in phase-change problems. Int J Numer Methods Eng 24(2):375–392
36. Tamma KK, Namburu RR (1990) Recent advances, trends and new perspectives via enthalpy-based finite element formulations for applications to solidification problems. Int J Numer Methods Eng 30(4):803–820
37. Tarzia DA (2011) Advanced topics in mass transfer, InTech, chap. 20, pp 439–484
38. Voller V, Cross M (1981) Accurate solutions of moving boundary problems using the enthalpy method. International J Heat Mass Transf 24(3):545–556
39. Wriggers P (2008) Nonlinear finite element methods. Springer, Berlin